Toughening and Compatibilization of Polypropylene/Polyamide-6 Blends with a Maleated–Grafted Ethylene-*co*-vinyl acetate

Hongzhi Liu,[1,3] Tingxiu Xie,[2] Lianlong Hou,[1,3] Yuchun Ou,[1] Guisheng Yang[1,2]

[1]*Key Laboratory of Engineering Plastics, Joint Laboratory of Polymer Science and Materials, Institute of Chemistry, Chinese Academy of Sciences, Beijing 100080, People's Republic of China*
[2]*Shanghai Genius Advanced Materials Co., Ltd., Beisong Road No. 800, Shanghai 201109, People's Republic of China*
[3]*Graduate School of the Chinese Academy of Sciences, Yuquan Road No. 19, Beijing 100049, People's Republic of China*

Received 17 March 2005; accepted 20 August 2005
DOI 10.1002/app.23006
Published online in Wiley InterScience (www.interscience.wiley.com).

ABSTRACT: In this article, maleated–grafted ethylene-*co*-vinyl acetate (EVA-*g*-MA) was used as the interfacial modifier for polypropylene/polyamide-6 (PP/PA6) blends, and effects of its concentration on the mechanical properties and the morphology of blends were investigated. It was found that the addition of EVA-*g*-MA improved the compatibility between PP and PA6 and resulted in a finer dispersion of dispersed PA6 phase. In comparison with uncompatibilized PP/PA6 blend, a significant reduction in the size of dispersed PA6 domain was observed. Toluene-etched micrographs confirmed the formation of interfacial copolymers. Mechanical measurement revealed that the addition of EVA-*g*-MA markedly improved the impact toughness of PP/PA6 blend. Fractograph micrographs revealed that matrix shear yielding began to occur when EVA-*g*-MA concentration was increased upto 18 wt %. © 2006 Wiley Periodicals, Inc. J Appl Polym Sci 99: 3300–3307, 2006

Key words: poly(propylene); polyamide-6; toughness; compatibilization

INTRODUCTION

Blending polypropylene (PP) with polyamides (PA) such as PA6 represents a versatile route to novel multiphase engineering resins, which combine high stiffness, strength, dimensional and environmental stability with high toughness and excellent processability. However, because of their immiscibility, addition of interfacial modifiers is required to achieve these advantages. For many years, following the early pioneering advances by Ide and Hasagawa,[1] maleic anhydride-grafted polypropylene (PP-*g*-MAH) has been used extensively for compatibilization of PP and PA6. In the melt, the maleic anhydride groups can easily react with the amine end groups of PA6 to *in-situ* form block or graft copolymers. These resulting copolymers efficiently reduce the interfacial tension between PP and PA6, thus, also reducing the size of dispersed PA6 phase and enhancing the mechanical properties of the blends. Despite some increase in both strength and stiffness, the impact strength does not improve markedly and fails to meet the requirements for applications of engineering resins. In the literature, maleated styrene–ethylene/butylene–styrene triblock copolymers (SEBS-*g*-MA),[2–14] EPM-*g*-MA,[8,9] ionomer,[15,16] and maleated thermoplastic elastomer (TPEg)[17–19] have been successfully used as both impact modifier and compatibilizer for PP/PA6 blends.

Ethylene-*co*-vinyl acetate grafted with maleic anhydride (EVA-*g*-MA) has been proven as an effective compatibilizer of PA6/EVA[20,21] and PBT/nylon-6[22] blends. On the other hand, unmodified EVA itself has also been applied to improve impact toughness of PP.[23,24] However, until now, there are few available reports related with EVA-*g*-MA as interfacial modifier of PP/PA6 blend. In this study, EVA-*g*-MA was added into PP/PA6 blends, and effects of EVA-*g*-MA concentration on the mechanical properties and the compatibilization were investigated. In addition, the morphologies of impact fracture surfaces were correlated with their impact strength.

EXPERIMENTAL

Materials

Polypropylene (PP2401) was purchased from Yanshan Petro. and Chem. (Beijing, China) with melt flow index (MFI) equal to 3.9 g/10 min (230°C, 2.16 kg). Polyamide-6 (PA6) was supplied by Shanghai Plastics

Correspondence to: Y. Ou, G. Yang (hzliu@iccas.ac.cn).
Contract grant sponsor: National Natural Science Key Foundation; contract grant number: 10032010.
Contract grant sponsor: National Natural Science Foundation; contract grant number: 10272005.

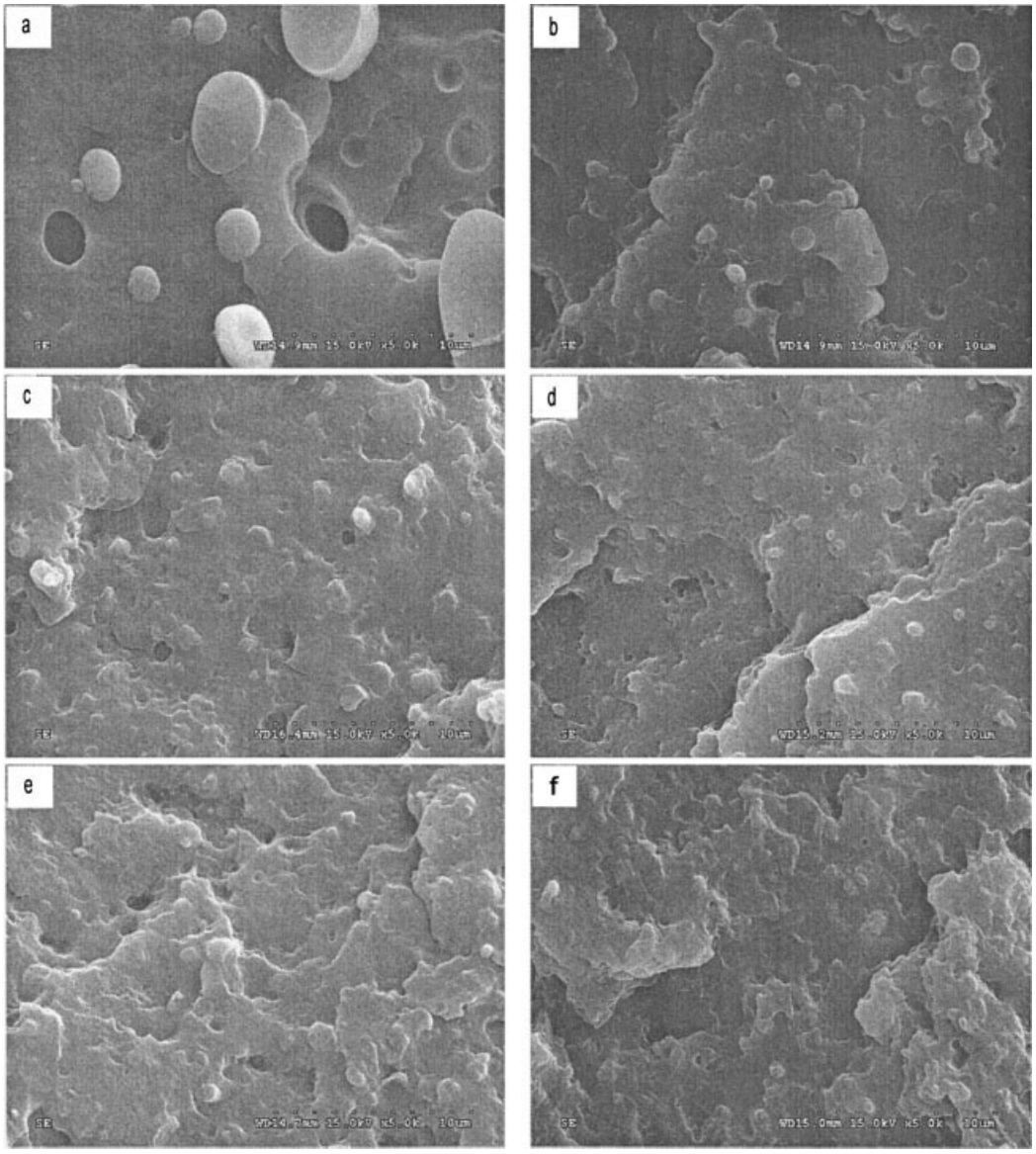

Figure 1 SEM micrographs of cryo-fractured surfaces of injection-molded PP/PA6/EVA-*g*-MA blends with different concentrations of EVA-*g*-MA: (a) 0 wt %; (b) 6 wt %; (c) 12 wt %; (d) 18 wt %; (e) 24 wt %; (f) 30 wt %.

Production Factory No. 18 (Shanghai, China) with the relative viscosity equal to 2.6–2.9. Maleic anhydride-grafted ethylene-*co*-vinyl acetate, designated as EVA-*g*-MA (MA graft ratio of 1 wt %), was kindly provided by Shanghai Zeming Plastics (Shanghai, China). Its MFI value and vinyl acetate content are 5.2 g/10 min (230°C, 2.16 kg) and 28 wt %, respectively.

Blend preparation

Before mixing, PA6 resin was dried for 12 h at 80°C to remove moisture. The PP/PA6 and PP/PA6/EVA-*g*-MA blends were prepared by melt extrusion, using a ϕ30mm-twin-screw extruder with an L/D ratio of 23.2 (SHJ-30, Nanjing Plastic Machinery, Nanjing, China) at 250 rpm. The content of PA-6 was fixed at 30 wt % in the above blends. The extruding temperature at various zones was between 180 and 230°C. The extruded strands were cooled immediately after extrusion in a water bath and then pelletized. Before injection molding, the pellets were dried at 80°C for12 h. For comparison, pure PP resin and PP/EVA-*g*-MA binary blends were also extruded under the above same condition.

Mechanical properties measurement

Specimens for mechanical properties measurement were prepared using a HTF80-W2 injection-molded machine (Ningbo Haitian, China). The temperature profiles for injection molding were 180–230°C at the different heating zones, and the mold temperature

was kept at 60°C. Before molding, the pellets were dried at 80°C for 8 h.

The tensile and flexural tests were performed with an Instron 3356 Universal Testing Machine according to GB1040–79 and GB1042–79 standards, respectively. The crosshead speeds for tensile and flexural tests are 50 and 2 mm/min, respectively. The Izod notched impact measurement was measured with an impact testing machine CSI-137C according to GB1843–80 standards.

Scanning electron microscopy

The scanning electron micrographs were recorded with a scanning electron microscope (SEM, Hitachi S-530) operating at an acceleration voltage of 15 kV. Prior to observation, the surfaces of the specimens were sputtered with gold to avoid electrical charging during examination.

To estimate the size of the dispersed PA6 domain in the blends quantitatively, the cryo-fractured surface is etched in formic acid, followed by a thorough rinse with anhydrous methanol. After vacuum-drying at ambient temperature, the etched fracture surfaces were also sputtered with gold prior to SEM observation. At least 200 particles from different micrographs of a specimen surface were analyzed to calculate the number–average diameter (d_n) and volume–average diameter (d_v) from the following relationships:

$$\bar{d}_n = \frac{\Sigma n_i d_i}{\Sigma n_i}$$

$$\bar{d}_v = \frac{\Sigma n_i d_i^4}{\Sigma n_i d_i^3}$$

where n_i is the number of particles having the particle diameter d_i.

Since the RuO_4-stained TEM micrographs cannot afford enough contrast between PP and EVA phases for compatibilized PP/PA6 blends, the selective-etched experiments were chosen to further allow a clear identification of phase morphologies of EVA-*g*-MA components. The specimens were freeze-fractured in liquid nitrogen and were then etched with toluene for 24 h at ambient temperature to dissolve EVA phase.[24–27]

RESULTS AND DISCUSSION

Compatibilizing effect of EVA-*g*-MA

Figure 1 shows micrographs of the cryogenically fractured cross sectioned surfaces for the PP/PA6 blend, compatibilized with various concentrations of EVA-*g*-MA. In the uncompatibilized PP/PA6 [Fig. 1(a)], the fracture surface is very smooth and large dispersed PA6 particles (4–6 μm in diameter) pulled away during the fracture process are clearly observed, which indicates the poor interfacial adhesion between PP and PA6. By contrast, the addition of EVA-*g*-MA improves the homogeneity of the blend morphology. In these compatibilized blends, the particles are embedded in the matrix. Again, the degree of adhesion seems to increase with the amount of added EVA-*g*-MAH and it is almost difficult to distinguish the dispersed phase.

Figure 2 further gives effects of EVA-*g*-MA concentration on number average and volume average diameters of dispersed PA6 particles. The plots exhibit the typical shape of an emulsification curve, as previously described by Favis: an initial rapid drop in particle size with EVA-*g*-MA concentration was observed up to a critical concentration (18 wt %), beyond which a quasi-equilibrium particle size is attained.[28] The 18 wt % critical concentration can be defined as the interface saturation concentration, beyond which the interface is saturated by the modifier.[29,30] More than 10- and 7-fold reduction in the values of d_v and d_n were observed, respectively. In addition, the particle size distribution, d_v/d_n, is reduced from 3.5 to 2.3, implying that the presence of EVA-*g*-MA results in a more homogeneous dispersion of PA6 particles in the PP matrix. The fine dispersion morphology upon incorporation of the interfacial modifier is mainly attributed to two different phenomena: a decrease of the interfacial tension and suppression of coalescence. Favis and coworkers[30] evaluated the relative roles of coalescence and interfacial tension in controlling dispersed phase size reduction during compatibilization, based on both emulsification curves and interfacial tension measurements. They showed that in the case of the PET/PP (99/1) blend, upon addition of SEBS-

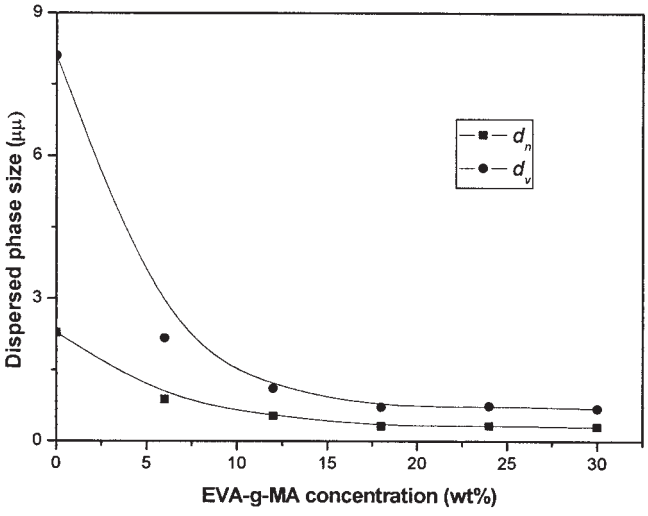

Figure 2 Volume average diameter (d_v) and number average diameter (d_n) as a function of EVA-*g*-MA content in PP/PA6/EVA-*g*-MA blends.

g-MA, the decrease of the dispersed phase size was caused only by a decrease in interfacial tension, whereas for PET/PP (90/10) blends, both the lowering of interfacial tension and suppression of coalescence were equally important in determining the reduction of dispersed phase size during compatibilization. In this case, the maleic anhydride group of EVA-*g*-MA reacts with the terminal amino group of PA6 during melt extrusion, as shown below (Scheme 1).

The *in-situ* formed EVA-*g*-PA6 copolymer is believed to locate the interphase between PP and PA6, which not only lowers their interfacial tension, but also suppresses the tendency of coalescence, thus resulting in a fine dispersion of PA6 particles. Simultaneously, it also improves interfacial adhesion between the components and facilitates the stress transfer during impact fracture, which is demonstrated by fracture surface morphologies.

To further clarify the phase structure in the compatibilized PP/PA6 blends, toluene was used to selectively etch out EVA-*g*-MA component of the blends, at room temperature. Both PP and PA6 are insoluble and thus, the selective etching may provide some information about the distribution of EVA-*g*-MA component. Figure 3 presents the micrographs of PP/PA6/EVA-*g*-MA blends after etching. Below EVA-*g*-MA concentration of 24 wt %, it can clearly be observed that the interface around some particles is etched to different extent. This should result from the formed EVA-*g*-MA interlayer via *in-situ* compatibilization between dispersed PA6 and PP matrix. With EVA-*g*-MA concentration increasing, the encapsulated PA6 particles become smaller, which is consistent with the above formic acid etched results. It is very interesting that the number of PA6 particles encapsulated seems to increase with EVA-*g*-MA concentration. Besides, one can find that some etched holes also exist inside some PA6 particles when the concentration of EVA-*g*-MA is less than 18 wt %. It suggests that some EVA-*g*-MA is likely to be entrapped in the PA6 phase during the process of compatibilization. However, when EVA-*g*-MA content is further increased, the etched parts begin to connect each other until the cocontinuous structure seems to be formed at the content of 30 wt % EVA-*g*-MA. Because EVA-*g*-MA is immiscible with PP matrix, this morphology may be caused by agglomeration of some unreacted EVA-*g*-MA phase dispersed in PP matrix when interfacial saturation is reached.

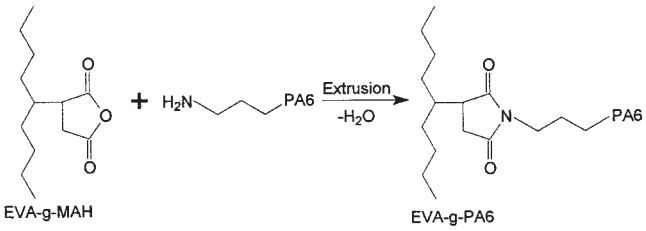

Scheme 1

Toughening effect of EVA-*g*-MA (mechanical properties)

Figure 4(a) shows stress–strain curves of PP/PA6/EVA-*g*-MA blends containing different EVA-*g*-MA concentration. The data from tensile and flexural measurement are listed in Table I.

The uncompatibilized PP/PA6 (70/30) blend exhibits very inferior strain at break (7.6%) and no noticeable yielding can be observed, which implies very poor interfacial adhesion between the blend components. When 6 wt % EVA-*g*-MA is added, a prominent yielding point can be observed and elongation at break increases by a factor of 4.3. On incorporation of EVA-*g*-MA up to 18 wt %, the compatibilized blend exhibits lower yield stress with broadening of the yield peak, accompanied by necking during elongation. With further increasing to 30 wt %, the yield point becomes unclear, accompanied by strain hardening. Elongation at break exhibits 41-fold increase, as compared with the uncompatibilized PP/PA6 blend. In this case, the stress–strain behaviors of the sample behave in a more or less rubber-like fashion. This supports the suggestion that the blend may contain an almost continuous network of agglomerated PA6 domains, enclosed in a rubbery interphase of partially grafted EVA-*g*-MA. The tensile fracture energy, i.e. the area of stress-strain curves, is usually used as a means of toughness. It can be found, from Table I, that the fracture energy of the blend increase remarkably with EVA-*g*-MA concentration. In addition, the addition of EVA-*g*-MA gradually decreases both strength and moduli of PP/PA6 blend, except 6 wt % concentration. This is evidently attributed to the elastic characteristics of the added EVA-*g*-MA.

For the sake of comparison, the deformation behaviors of the corresponding PP/EVA-*g*-MA binary blends are shown in Figure 4(b). The tensile and flexural properties are listed in Table I. In all these curves, the binary blends undergo typical yielding deformation and necking in a manner resembling that of pure PP, although the yield stress was lowered. As is expected, the flexural moduli and strength of PP/EVA-*g*-MA binary blends decrease with increasing EVA-*g*-MA content. However, as EVA-*g*-MA concentration increases, both elongation at break and tensile fracture energy of PP/EVA-*g*-MA blends are still below those of pure PP resin. This tendency is quite different from that of the aforementioned PP/PA6/EVA-*g*-MA blends.

The notched Izod impact strength of PP/PA6/EVA-*g*-MA and PP/EVA-*g*-MA blends as a function of EVA-*g*-MA concentration is shown in Figure 5. When

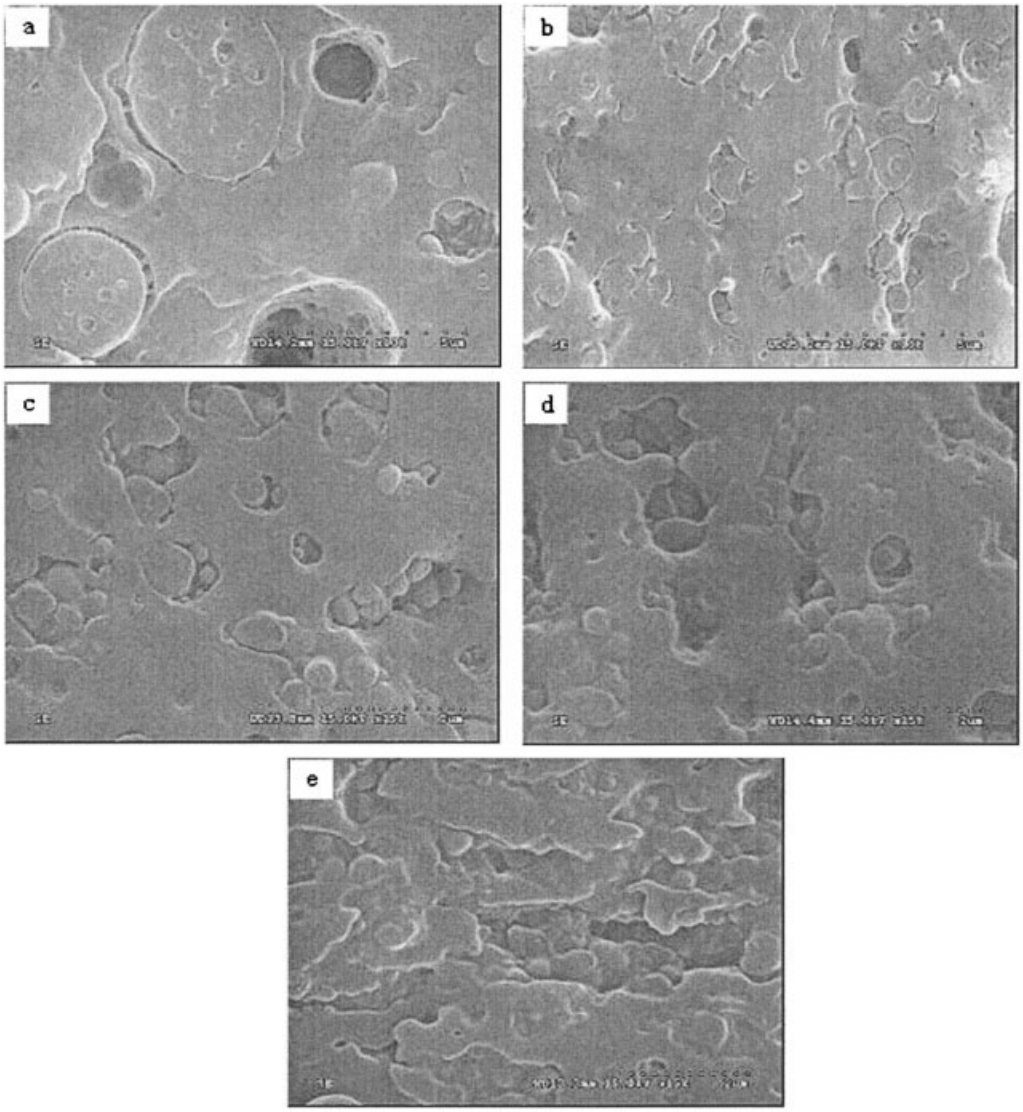

Figure 3 Toluene-etched scanning electron micrographs of PP/PA6/EVA-*g*-MA blends: (a) 64/30/6; (b) 58/30/12; (c) 52/30/18; (d) 46/30/24; (e) 40/30/30.

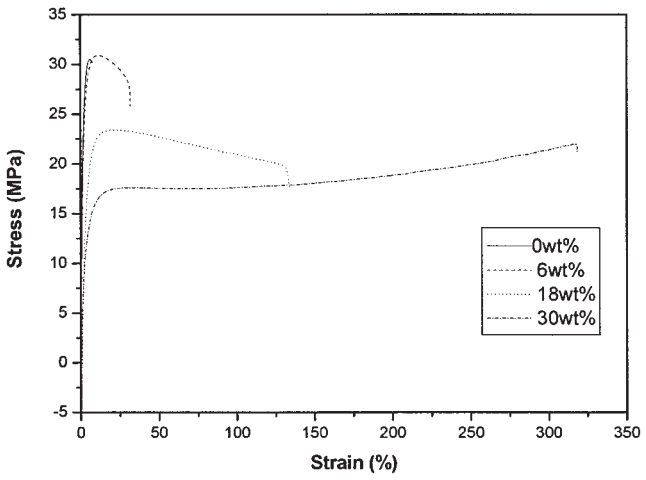

Figure 4 Influence of added EVA-*g*-MA concentration on stress–strain behaviors of PP/PA6 blends.

6 wt % EVA-*g*-MA is added, the impact toughness of both PP/PA6/EVA-*g*-MA and PP/EVA-*g*-MA blends is almost the same. Beyond this concentration, however, toughness is improved more rapidly for compatibilized PP/PA6 blends than the corresponding PP/EVA-*g*-MA blends. In case of the former blend system, such an improvement of toughness is especially evident when EVA-*g*-MA concentration exceeds 24 wt %. By contrast, PP/EVA-*g*-MA blends exhibit a very slight increase in impact strength with EVA-*g*-MA content. Compared with pure PP resin, about threefold increases are achieved for PP/EVA-*g*-MA binary blend containing 30 wt % EVA-*g*-MA. On the basis of the discussion, the toughness enhancement of PP/PA6/EVA-*g*-MA blends mainly results from the compatibilizing role of EVA-*g*-MA. Like PP/PA6/EVA-*g*-MA blends, the strength and moduli of PP/

TABLE I
Mechanical Properties of PP/PA6/EVA-*g*-MA and PP/EVA-*g*-MA Blends

EVA-*g*-MA concentration (wt %)	Tensile strength (MPa)	Elongation at break (%)	Flexual strength (MPa)	Flexural modulus (MPa)	Tensile fracture energy (J)
PP/PA6/EVA-*g*-MA					
0	29.5	7.6	38.0	1085	4.1
6	30.9	32.9	36.3	991	20.6
12	27.1	95.7	30.3	806	47.8
18	23.8	114.4	25.8	670	53.7
24	21.5	256.0	21.4	569	114.3
30	21.8	314.2	16.8	434	125.6
PP/EVA-*g*-MA					
0	29.1	612	37.1	1067	285
6	28.5	460	33.2	985	196
12	25.5	527	28.9	838	211
18	24.2	484	26.4	743	184
24	22.5	619	24.6	707	219
30	20.4	669	21.9	623	234

EVA-*g*-MA blends decrease upon the increase of EVA-*g*-MA content.

Fractography

The impact fracture processes of a solid polymer material are well reflected in the appearance of the fracture surface.[31] Observation of the fracture surface helps us to understand the involved impact energy dissipation mechanisms upon impact testing. Figure 6 shows SEM fractographs of PP/PA6 and PP/PA6/EVA-*g*-MA blends. In the case of uncompatibilized PP/PA6 blend [Figs. 6(a,b)], the dispersed phase are rather rough and the interfacial adhesion is very weak, which is attributed to the poor compatibility between PP and PA6. The fracture surface is very smooth, typical of a brittle failure. Despite the increased interfacial adhesion, the addition of 6 wt % EVA-*g*-MA only shows very limited cavitations. Now, it is generally believed that shear yielding of the matrix is the major energy-absorbing mechanism and therefore, the impact toughness is not improved in this case [Figs. 6(a,b)]. When EVA-*g*-MA concentration is increased to 18 wt %, the fracture surface changes remarkably and exhibits matrix shear yielding beyond the notch [Fig. 6(f)]. Kim et al. studied toughening mechanisms occurring in various toughened and particle filled semicrystalline polymers.[32,33] They pointed out that although void formation, followed by cavitations or debonding process, itself is a secondary factor contributing to toughness, it plays an important role for the activation of further plastic deformation of matrix materials during the micromechanical deformation process. Once the microvoid is formed in the matrix, the hydrostatic stress caused by stress concentration is released and the shear stress is lowered. The constrained conditions, i.e. triaxial stresses, disappear and the matrix behaves as if it was under plane stress conditions. Shear yielding deformations occur more readily under a biaxial stress state rather than the craze-favoring triaxial state.

With further increasing EVA-*g*-MA concentration to 30 wt %, the matrix yielding becomes more extensive and elongated matrix ligaments can be visible. Such fracture mechanism dissipates a significant amount of impact energy and thus, impact toughness is improved remarkably.

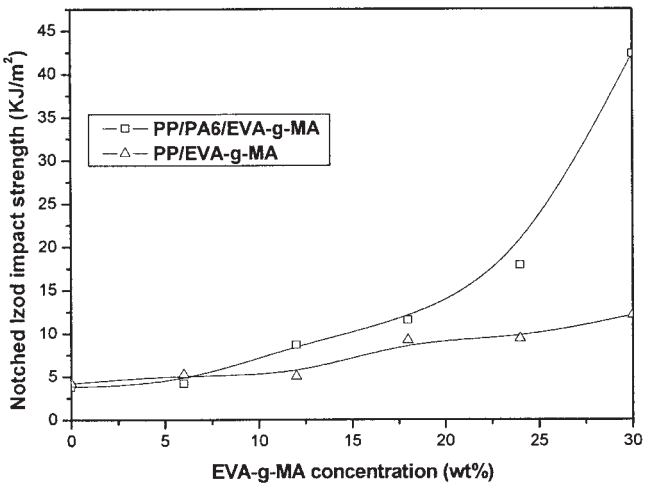

Figure 5 Variations of notched Izod impact strength of PP/PA6/EVA-*g*-MA and PP/EVA-*g*-MA blends with EVA-*g*-MA concentration, respectively.

CONCLUSIONS

In this study, the different concentration of EVA-*g*-MA was added into uncompatibilized PP/PA6 blends with a

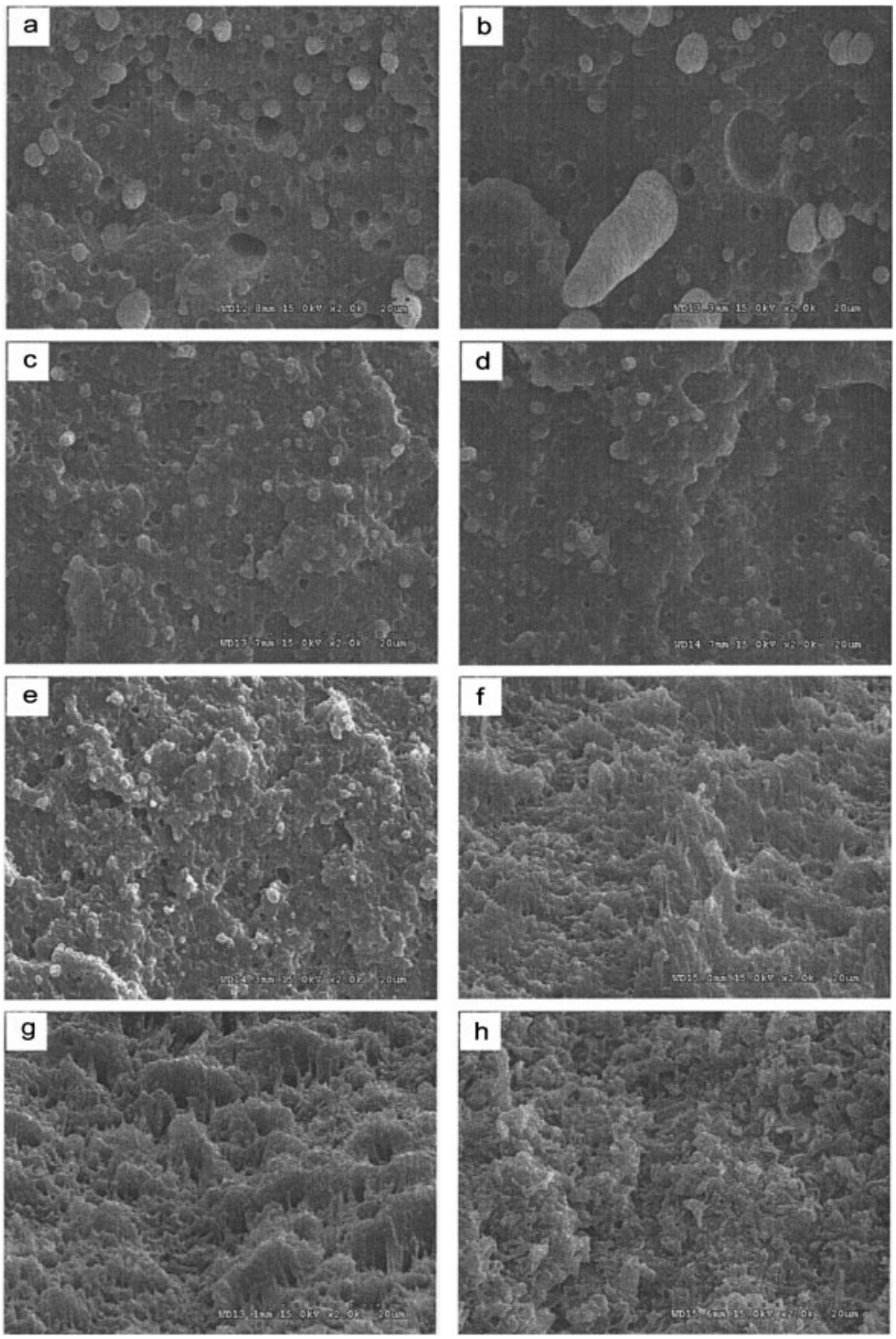

Figure 6 Scanning electron micrographs of impact-fractured surface of PP/PA6/EVA-*g*-MA blends containing: (a,b) 6 wt %; (c,d) 12 wt %; (e,f) 18 wt %; (g,h) 30 wt %. (Left photographs: near notch, right photographs: beyond notch).

fixed PA6 content (30 wt %) as interfacial modifier. Mechanical properties, freeze-fractured morphology, and fractography of ternary blends were investigated. SEM observations suggest that, a fine dispersion and good interfacial adhesion were achieved with the addition of EVA-*g*-MA. The size of dispersed PA6 particles initially decreased rapidly with increasing EVA-*g*-MA concentration, followed by a steady particle size being achieved. Compared with the uncompatibilized PP/PA6 blend, an overall 10-fold decrease in d_v was achieved and the size distribution also became narrow. The toluene-etched scanning electron micrographs confirm the presence of *in-situ* forming EVA interphase between PP and PA6.

Mechanical properties demonstrated that, the addition of EVA-*g*-MAH considerably improved the toughness of PP/PA6 blends. Impact-fracture mor-

phology of PP/PA6/EVA-*g*-MA blends revealed that, matrix shear yielding began to appear beyond the notch, when EVA-*g*-MA concentration reaches 18 wt %. Further increasing of EVA-*g*-MA concentration led to an extensive matrix yielding, which became the main mechanism of the impact energy dissipation upon impact testing. On the contrary, the addition of EVA-*g*-MA failed to improve the toughness of PP resin.

References

1. Ide, F.; Hasagawa, A. J Appl Polym Sci 1974, 18, 963.
2. Ikkala, O. T.; Holsti-Miettinen, R. M.; Seppala, J. J Polym Sci Part B: Polym Phys 1993, 49, 1165.
3. Holsti-Miettinen, R. M.; Seppala, J.; Ikkala, O. T. Polym Eng Sci 1992, 32, 868.
4. Wilkinson, A. N.; Laugel, L.; Clemens, M. L.; Harding, V. M.; Marin, M. Polymer 1998, 40, 4971.
5. Wilkinson, A. N.; Clemens, M. L.; Harding, V. M. Polymer 2004, 45, 5239.
6. Rösch, J.; Mülhaupt, R. Makromol Chem Rapid Commun 1993, 14, 503.
7. Rösch, J. Polym Eng Sci 1995, 35, 1917.
8. Rösch, J.; Mülhaupt, R. Polym Bull 1994, 32, 697.
9. Rösch, J.; M[mul]ulhaupt, R.; Michler, G. H. Macromol Symp 1996, 112, 141.
10. Kim, G.-M.; Michler, G. H.; Rüsch, J.; Mülhaupt, R. Acta Polym 1998, 49, 88.
11. Kim, G.-M.; Michler, G. H.; Gahleitner, M.; Mülhaupt, R. Polym Adv Technol 1998, 9, 709.
12. Tasdemir, M. J Appl Polym Sci 2003, 89, 3485.
13. Ohlsson, B.; Hassander, H.; Törnell, B. Polymer 1998, 39, 4715.
14. Ohlsson, B.; Hassander, H.; Törnell, B. Polymer 1998, 39, 6705.
15. Willis, J. M.; Favis, B. D. Polym Eng Sci 1988, 28, 1416.
16. Willis, J. M.; Caldas, V.; Favis, B. D. J Mater Sci 1991, 26, 4742.
17. Ou, Y.-C.; Lei, Y.-G.; Fang, X.-P.; Yang, G.-S. J Appl Polym Sci 2004, 91, 1806.
18. Liu, H.-Z.; Xie, T.-X.; Ou, Y.-C.; Fang, X.-P.; Yang, G.-S. Polym J 2004, 36, 754.
19. He, A.-H.; Ou, Y.-C.; Fang, X.-P.; Liu, H.-Z. Acta Polym Sin 2004, 4, 534.
20. Bhattacharyya, A. R.; Ghosh, A. K.; Misra, A.; Eichhorn, K.-J. Polymer 2005, 46, 1661.
21. Bhattacharyya, A. R.; Ghosh, A. K.; Misra, A. Polymer 2001, 42, 9143.
22. Kim, S.-J.; Kim, D.-K. Polym Eng Sci 2003, 43, 1298.
23. Gupta, A. K.; Ratnam, B. K.; Srinivasan, K. R. J Appl Polym Sci 1992, 45, 1303.
24. Jafari, S. H.; Gupta, A. K. J Appl Polym Sci 2000, 78, 962.
25. Marguerat, F.; Carreau, P. J.; Michel, A. Polym Eng Sci 2002, 42, 1941.
26. Maciel, A.; Del-Real, A.; Garcia-Garduno, M. V.; Oliva, E.; Manero, O.; Castano, V. M. Polym Int 1996, 41, 227.
27. Pimbert, S.; Stevenson, I.; Seytre, G.; Boiteux, G.; Cassagnau, P. Macromol Symp 2005, 222, 239.
28. Favis, B. D. Polymer 1994, 35, 1552.
29. Lepers, J.-C.; Favis, B. D.; Lacroix, C. J Polym Sci Part B: Polym Phys 1999, 37, 939.
30. Lepers, J.-C.; Favis, B. D.; Tabar, R. J. J Polym Sci Part B: Polym Phys 1997, 35, 2271.
31. Yu, Z. Z.; Lei, M.; Ou, Y. C.; Yang, G. S. Polymer 2002, 43, 6993.
32. Kim, G. M.; Michler, G. H. Polymer 1998, 39, 5689.
33. Kim, G. M.; Michler, G. H. Polymer 1998, 39, 5699.